
Chapter 7

DLC structures from RF magnetron sputtering

Chapter 7 – DLC structures from RF magnetron sputtering

7.1. Deposition rate

Me/a-C nanometric multilayer coatings have been prepared by sequential magnetron sputtering of metal and graphite targets. In a preliminary study, a series of DLC films have been deposited by RF magnetron sputtering on c-Si substrates at floating potential, either in continuous wave mode (CW) or in pulsed mode by square-wave modulation of the RF signal (SQWM) at 100 Hz frequency and 20% duty cycle, at different values of gas pressure and RF power. Both monolithic and multilayered structures were characterised and their properties have been compared.

Figure 7.1 shows that the deposition rate of the DLC films grown in CW decreases from 6 to 2 nm/min as the Ar gas pressure is increased from 0.2 to 2 Pa. RF power has been fixed to 300 W.

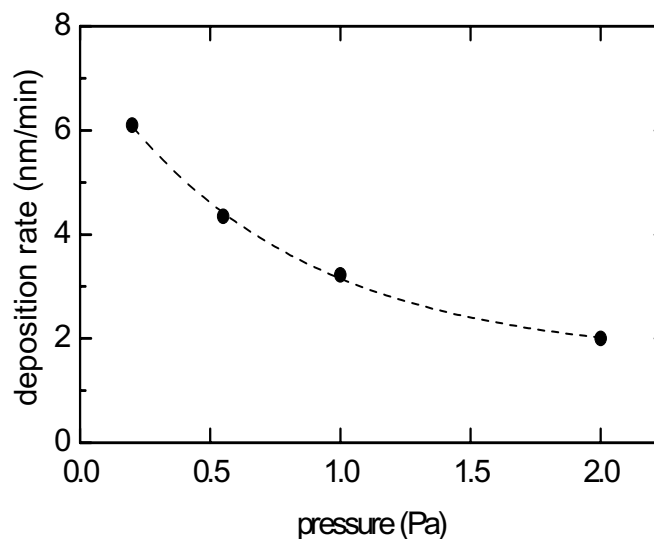


Figure 7.1: Dependence of deposition rate of a-C films on Ar gas pressure at 300 W of RF power.

The RF power dependence of deposition rate of DLC films at a constant pressure of 0.2 Pa is shown in figure 7.2. In the CW mode, the deposition rate rises from 1 to 6 nm/min with increasing RF power from 100 to 300 W. The enhancement of deposition rate as the RF power increases is also observed in the SQWM variant.

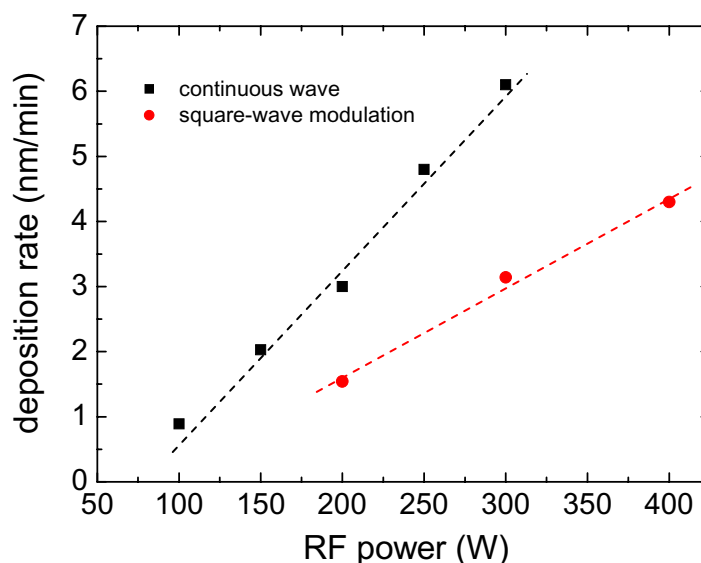


Figure 7.2: Deposition rate of DLC films as a function of RF power in CW, and RF power peak in the case of SQWM, at a fixed pressure of 0.2 Pa.

The growth of DLC films from sputtering of a graphite target by Ar ions consists of three main stages: (a) the ejection of sputtered C atoms (mostly neutral) at energies of approximately 10 eV; (b) the transport of these species through the plasma from the target to the substrate; and (c) their arrival and condensation onto the growing film surface. Both the sputtering pressure and the RF power discharge have a great influence on each of these stages [Andújar J.L., 2002].

The increase in RF power at constant pressure leads to an increase of the plasma electron density, which enhances the flow of Ar ions bombarding the target. In addition, the negative self-bias voltage on the target is raised, thus increasing the bombarding ion energy. As a consequence, the flow of sputtered C atoms is enhanced, leading to an increase in film deposition rate with increasing RF power, as shown in figure 7.2.

At low pressure (0.2 Pa), the mean free path of sputtered C atoms travelling through Ar gas is approximately a half of the target-substrate distance (65-70 mm), as calculated with equation 3.3. In this case, the sputtered atoms can reach the growing surface by losing energy in only one gas collision in average. However, as the pressure is increased, both the electron temperature and the electron density decrease [Rosnagel S.M., 1987]. In addition, and according to equation 3.3, the mean free path for both C and Ar atoms scales inversely with pressure. This results in major scattering and earlier thermalisation of these species by

collisions with the resident gas and, thus, to lower energy deposition conditions. These effects might account for the observed decrease of deposition rate with increasing pressure, shown in figure 7.1.

Monolithic films of W have also been deposited in order to know the deposition rate and mechanical properties of each multilayer component. Table 7.1 lists the deposition parameters of the single layers. Afterwards, four multilayer structures consisting of 15 W/a-C bilayers with a fixed W-layer thickness of 4 nm were prepared. The a-C layer grown under CW mode was 9 nm thick (sample CW). The multilayers prepared under SQWM conditions (samples PM-1, -2 and -3) had a-C layers of 12, 8 and 4 nm, respectively. Table 7.2 gives the characteristic parameters of such multilayers.

Sample	Mode	Pressure (Pa)	RF power (W)	Frequency (Hz)	Duty cycle (%)	Growth rate (nm/min)
W	CW	0.2	50	-	-	13
a-C	SQWM	0.2	300	30	30	3
a-C	CW	0.2	100	-	-	4

Table 7.1: Parameters of W and DLC single layers.

Sample	Mode	a-C thickness (nm)	Multilayer period (nm)	Total thickness (nm)
W/a-C CW	CW	9	13	200
W/a-C PM-1	SQWM	12	16	240
W/a-C PM-2	SQWM	8	12	180
W/a-C PM-3	SQWM	4	8	120

Table 7.2: Parameters of multilayers composed of 15 W/a-C bilayers. The thickness of each W layer was 4 nm.

Besides the structures described above, multilayered films consisting of 30 bilayers with a maximum total thickness of 100 nm have been also deposited. The deposition time of each a-C layer was 30 s, and the metallic layers were grown during 20 s per layer. Moreover, the substrates were biased within a range from -40 to -300 V when depositing a-C layers, in order to modify the bombardment energy, whereas the floating potential was selected for the metal layer growth. The pressure varied between 0.2 and 2 Pa. Table 7.3 lists the deposition conditions of these multilayer structures along with thickness and multilayer period.

Sample	Bias voltage (V)	Pressure (Pa)	Multilayer period (nm)	Total thickness (nm)
PM 11-0	-40	0.2	2.8	85
PM 11-1	-40	1	3.2	96
PM 12-1	-40	2	2.3	70
PM 12-2	-300	2	1.2	37
PM 12-3	-300	0.2	1.0	30
PM 12-4	-170	1	1.7	52
PM 12-5	-40	0.2	2.6	79

Table 7.3: Deposition conditions of W/a-C multilayer structures composed of 30 bilayers, where a-C layers were deposited by SQWM conditions and W by CW.

The deposition rate values of the multilayer systems of table 7.3 have been compared by taking into account the pressure, P , and the negative bias voltage, V_b , applied during the growth of each a-C layer. In the studied range, the dependence of the deposition rate on both parameters was practically linear, as shows the plot of the experimental deposition rate, R_d (figure 7.3).

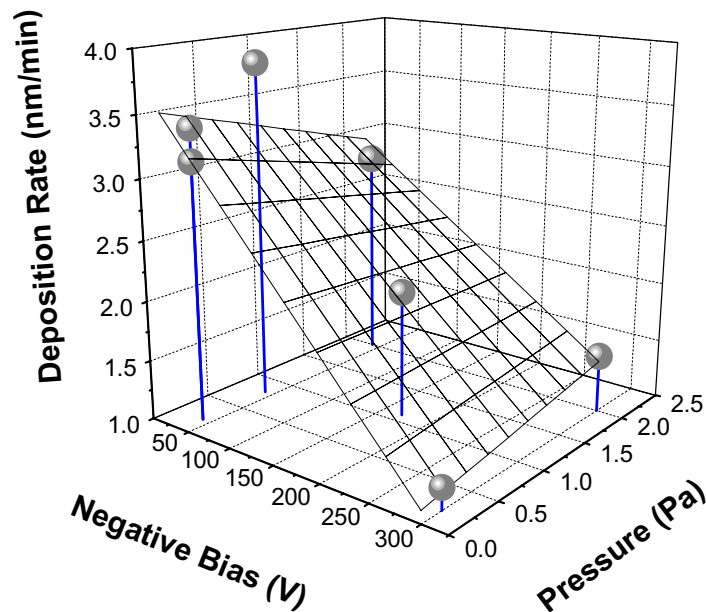


Figure 7.3: Plot of the experimental deposition rate points vs. the primary parameters: pressure during the process and bias voltage for W/a-C multilayer structure.

From the experimental data, an empirical model appropriated for the ranges of figure 7.3 has been calculated [Bertran E., 2003]:

$$R_d(P, V_b) = k_0 + k_1 V_b + k_2 P + k_3 V_b P \quad (7.1)$$

where the coefficients take the values: $k_0=6.33 \cdot 10^{-2}$ nm/s; $k_1=-5.67 \cdot 10^{-3}$ nm/(s·V); $k_2=-1.5 \cdot 10^{-4}$ nm/(s·Pa), and $k_3=2.83 \cdot 10^{-5}$ nm/(s·V·Pa). This dependence indicates that the growth of W/a-C multilayer structures is mainly limited by the bias voltage applied to the substrate during the deposition of a-C. This model also reveals an antagonistic behaviour depending on the bias voltage. At low bias, the deposition rate of the multilayer structures decreases with pressure, essentially due to the effect of Ar pressure on the efficiency of the sputtering process. On the other hand, the films grow faster at higher pressures at -300 V self-bias.

7.2. Raman spectroscopy

Visible Raman spectra of the DLC films are plotted in figure 7.4, and show two broad bands ascribed to the D and G peaks of sp^2 bonded carbon. Unlike the analysis of Raman spectra made in chapter 6, here these spectra were deconvoluted by using two Gaussian curves. Thus, the considered value of $I(D)/I(G)$ is not defined as the ratio of the peak heights any longer (chapter 6), but the ratio of the relative integrated intensity (Gaussian areas) of the D and G bands [Ferrari A.C., 2000].

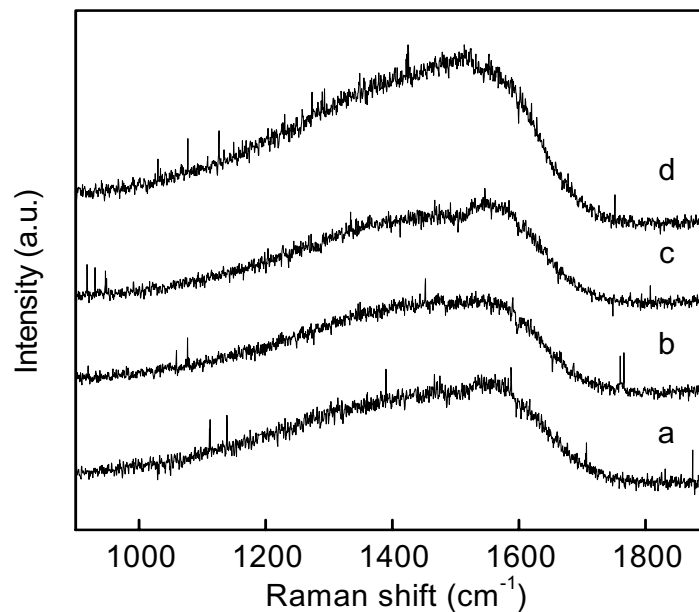


Figure 7.4: Raman spectra of sputter deposited DLC films grown at (a) 100 W RF power and 0.2 Pa pressure; (b) 200 W and 0.2 Pa; (c) 300 W and 0.2 Pa; and (d) 300 W and 2 Pa.

Figure 7.5 shows the Raman spectra of the DLC films grown under both continuous wave and pulsed modes. The spectra are quite similar, with the G-band centred at 1556 cm^{-1} and the D-band at around 1377 cm^{-1} . The intensity ratios of D-band to G-band are close to unity.

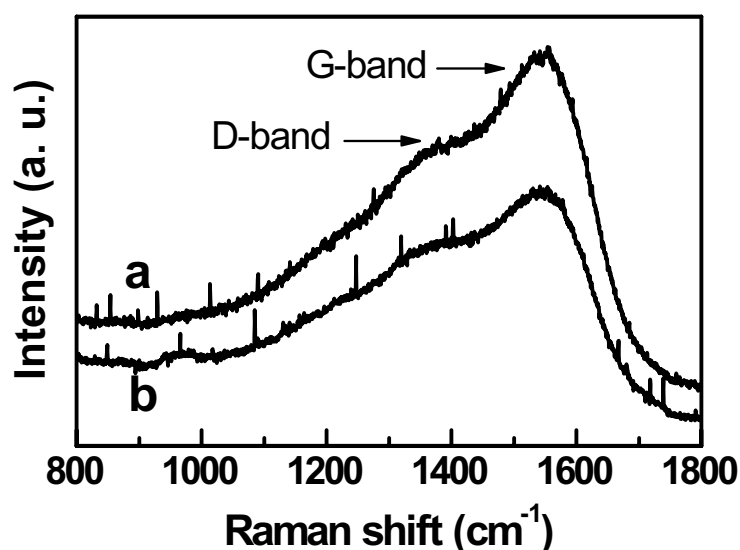


Figure 7.5: Raman spectra corresponding to sputter deposited DLC single-layer films grown (a) in CW mode and (b) in SQWM mode RF discharges.

As shown in figure 7.6, $I(D)/I(G)$ decreases and the center of the G band is shifted to lower wavenumbers with increasing Ar gas pressure. In a recent Raman study of amorphous carbon, a three-stage model has been proposed for the interpretation of Raman spectra [Ferrari A.C., 2000]. In the stage 2 of this model, the increase in the $I(D)/I(G)$ ratio together with the up-shift of the G peak position has been associated with an increase in the number and clustering of sp^2 sites into ordered rings. According to this interpretation, the results shown in figure 7.6 suggest that increasing pressure favours disordering of the sp^2 phase.

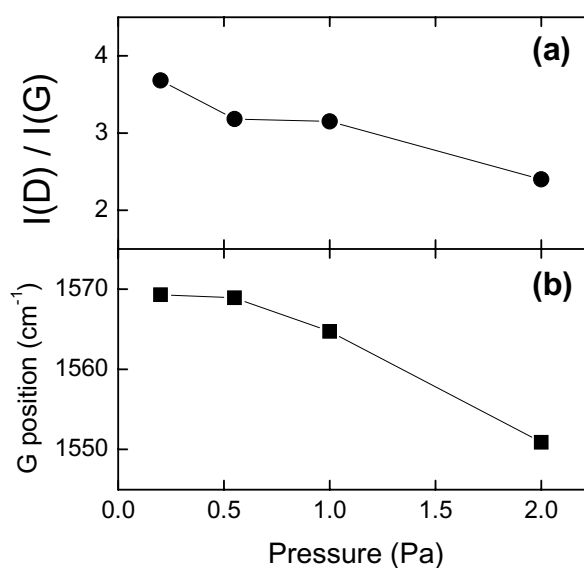


Figure 7.6: Pressure dependences of (a) $I(D)/I(G)$ and (b) G band wavenumber position, corresponding to DLC films grown at 300 W RF power.

As observed in the RF power influence at constant pressure, different patterns are observed in the case of CW and SQWM films in figure 7.7. In the CW mode, both the $I(D)/I(G)$ ratio and the G peak position first decrease with the increase in RF power. Afterwards, they reach a minimum at approximately 150 W, and then increase at higher RF power values. In contrast, the films grown in the SQWM mode show a slight increase of the $I(D)/I(G)$ ratio and the G peak position as the RF power is raised, with values below than those of CW mode.

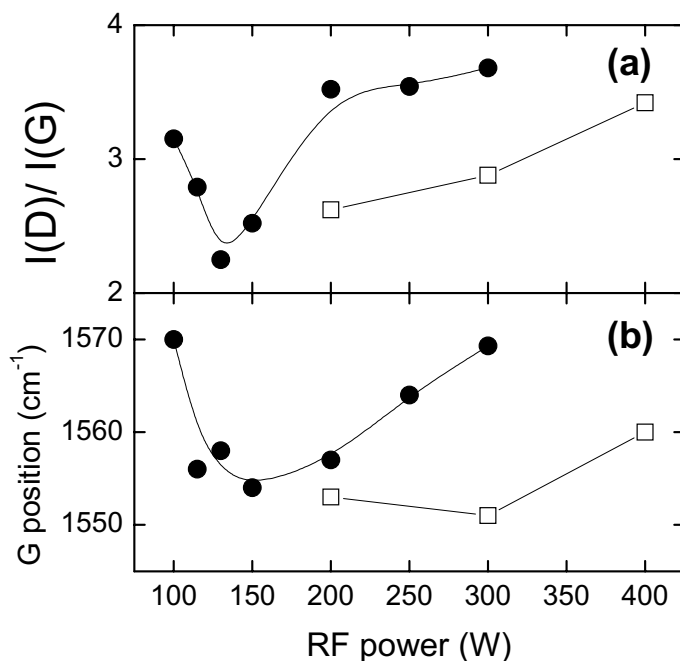


Figure 7.7: RF power dependence of (a) $I(D)/I(G)$ and (b) G band wavenumber position at a constant pressure of 0.2 Pa. Solid symbols correspond to a-C films grown in continuous wave mode, while open symbols correspond to those grown in SQWM mode, where RF power peak has been considered.

Following the interpretation of Ferrari et al. [2000], it appears that the increase of power in CW first leads to a reduction and then to an increase in ordered sp^2 clusters. Such behaviour could be ascribed to two competitive mechanisms induced by increasing power, namely, the enhancement of Ar ion bombardment in the low power region that favours the formation of diamond-like films, and the increase in the growing surface temperature at high power resulting in a graphitisation of the sp^2 domains.

7.3. Transmission electron microscopy: multilayer viewing

Figure 7.8 shows a cross-section bright-field TEM micrograph of the W/a-C multilayer PM-1 [Pinyol A., 2002]. A regular multilayer structure with sharp interfaces is observed. It contains 15 W/a-C bilayers sequentially deposited, whose alternated contrast is originated mainly by the difference in mass density between the carbon layer (bright) and tungsten layer (dark). The total thickness is 240 nm. A multilayer period of 16 ± 2 nm was estimated, where 12 ± 1 nm thickness corresponds to the a-C layers and 4 ± 1 nm thickness corresponds to the W layers.

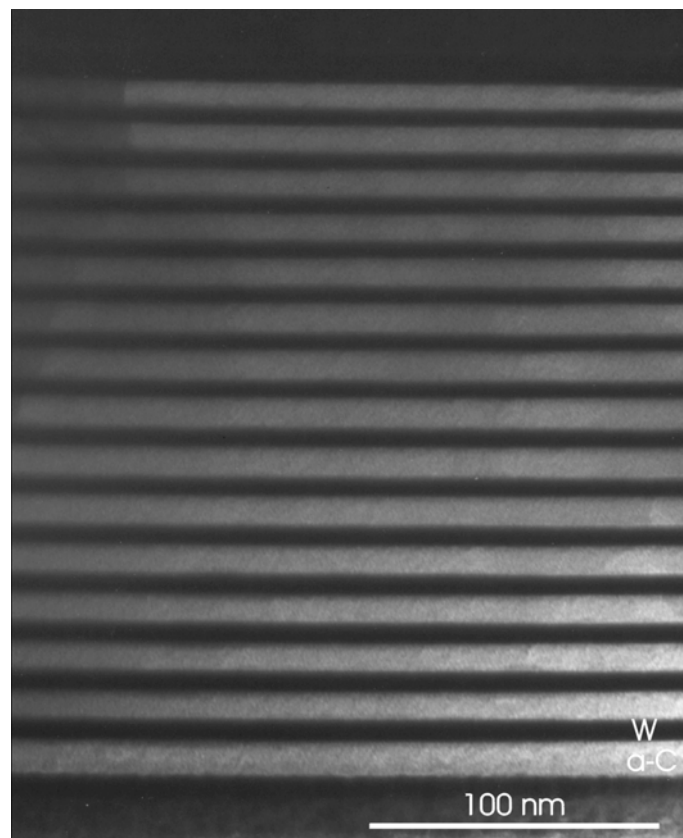


Figure 7.8: Cross-section TEM micrograph of a W/a-C multilayer with 15 bilayers. Bilayer thickness is 16 ± 2 nm.

The regular 30-bilayer structure corresponding to sample PM 11-1 is observed with sharp interfaces in the TEM image of figure 7.9. From this figure, a multilayer period of 3.5 ± 0.5 nm can be estimated corresponding to a total film thickness of 105 ± 15 nm.

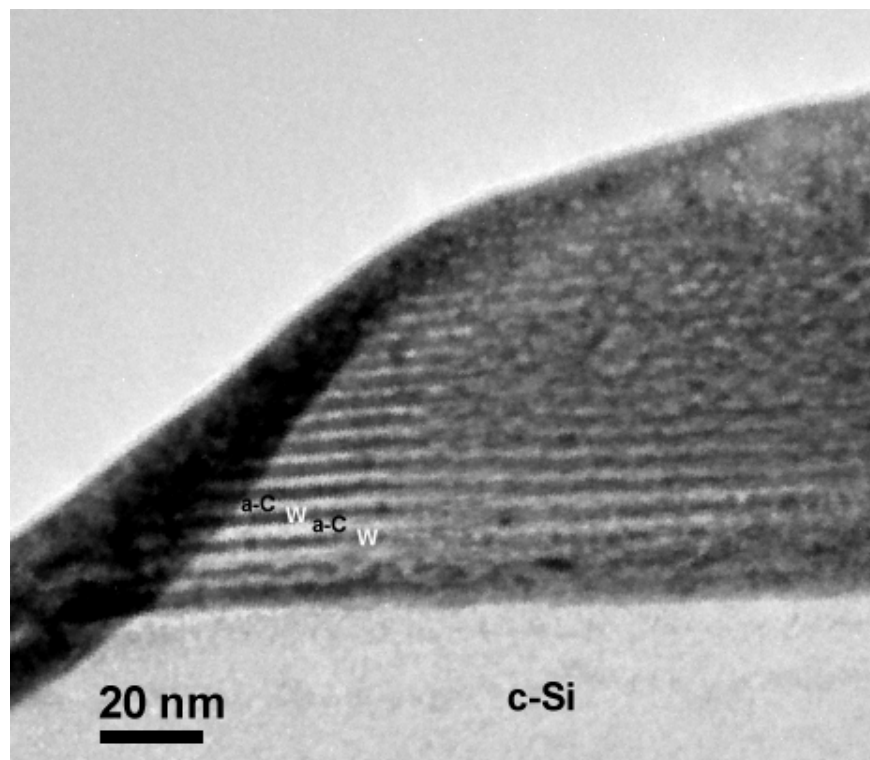


Figure 7.9: Cross-section TEM micrograph corresponding to a W/a-C multilayer structure of 30 bilayers with an estimated multilayer period of 3.5 ± 0.5 nm.

7.4. X-ray diffraction: crystal formation

Figure 7.10 shows the XRD diffractogram of the W film (W 010504-1), which is 380 nm thick. Diffraction peaks corresponding to both α and β phases of tungsten are pointed out. The β -W phase corresponds to a metastable phase of W, whereas the presence of the α -W phase is expected in sputtering deposition processes carried out at high temperature. It is true that substrates were air-cooled, but it was an inefficient cooling mechanism due to the large contribution to substrate heating of energetic neutrals from W target sputtering [Bewilogua K., 2000].

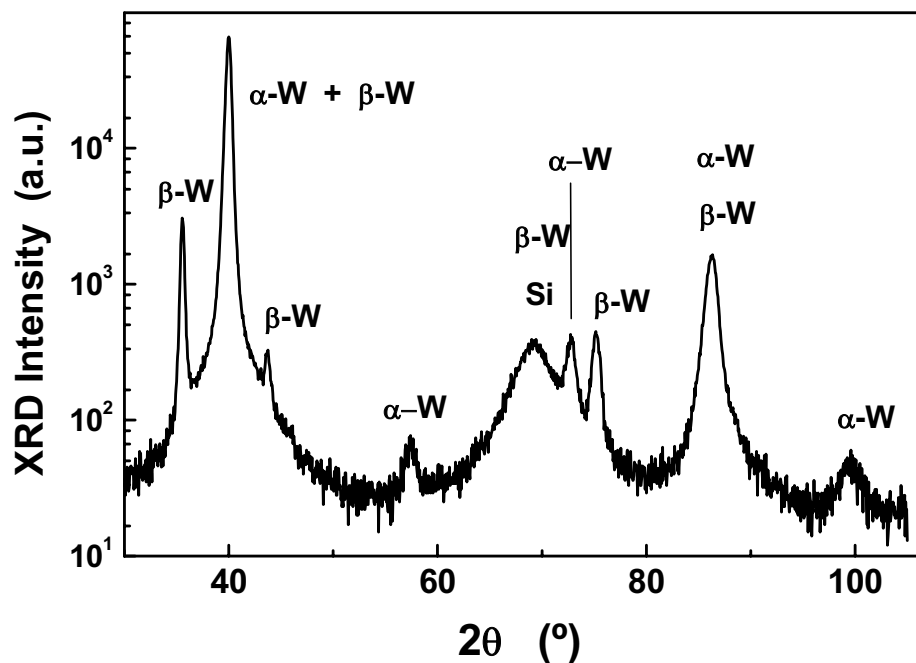


Figure 7.10: XRD diffractogram of a W single layer (W 010504-1).

W and DLC layers have been assembled in W/a-C structures by depositing them with the same experimental conditions as in the case of monolithic layers. Thus, the W/a-C multilayers are expected to show the peaks collection coming from α and β phases when analyzed by XRD. Instead of this, only two wide peaks were detected as show the XRD diffractogram of a W/a-C multilayered structure (sample PM-1) in figure 7.11. The peak located close 69° is identified as a reflection from the silicon substrate $\{100\}$, and it may account also for the (321) plane family from β -W. The maximum at 38.5° can be a composition of the contributions from α -W (110) and β -W (200), (210).

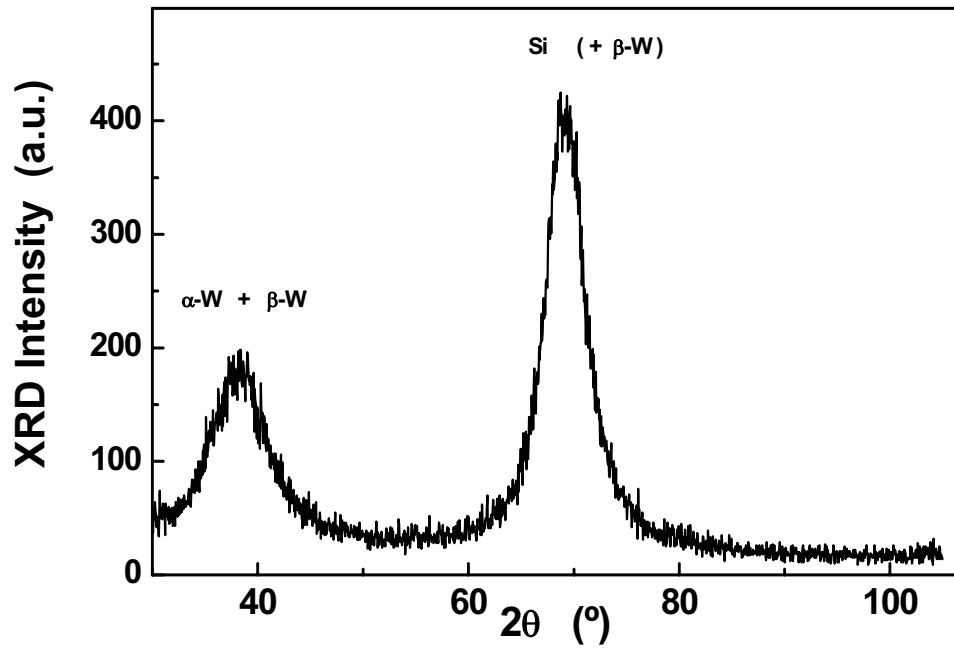


Figure 7.11: XRD diffractogram of a W/a-C multilayer film.

We can conclude that the crystallinity is weakened for so thin W layers. In fact, the fast compositional modulation during multilayer deposition can restrict the formation of new crystals in the W matrix. Thus, we infer that crystal formation is possible from a minimal multilayer period threshold. A similar phenomenon of crystal phase quenching has been observed in Me-DLC films, as described in chapter 8.

7.5. X-ray reflectivity: superlattice characterisation

The low-angle XRD (LAXRD) or XRR diffractogram of the multilayer PM-1 is shown in figure 7.12. The multilayer structure with repeating bilayer units produces the observed superlattice spectrum at low angles, as a result of the periodical modulation of electron density [Pinyol A., 2002]. This superlattice becomes measurable because the multilayer period is of the order of 10 nm. A high reflectivity appears at low angles, which is due to the structure of alternating high- and low-density layers.

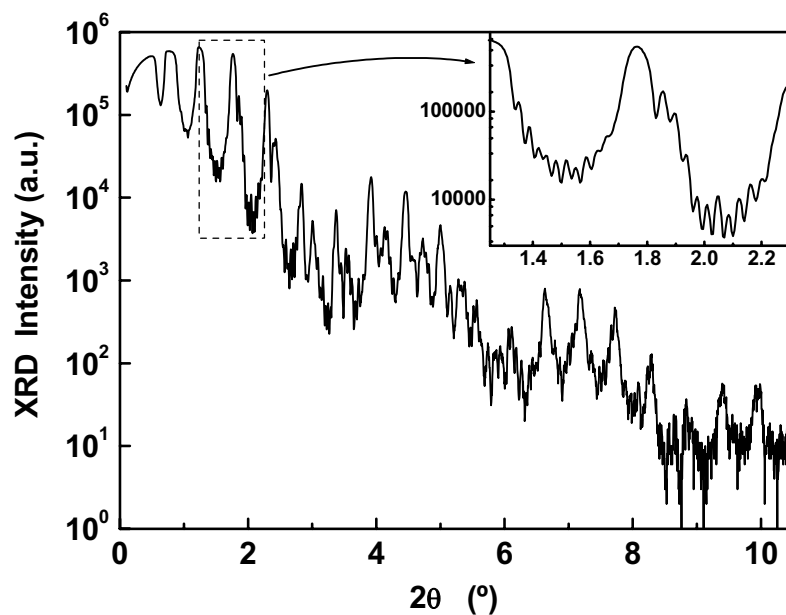


Figure 7.12: XRR diffractogram of a W/a-C multilayer.

From the XRR diffractogram, the bilayer thickness of the multilayer can be evaluated. Indeed, the angular position of the peaks, θ , obeys the modified Bragg's law [Agarwal B.K., 1979]:

$$\sin^2 \theta = \sin^2 \theta_C + \sin^2 \theta_B \quad (7.2)$$

where θ_C is the critical angle and θ_B corresponds to the position of the normal (high angle) Bragg peaks given by:

$$\sin \theta_B = \frac{n\lambda}{2\Lambda} \quad (7.3)$$

where n is the major-peak order, λ is the wavelength of the incident radiation (0.15406 nm), and Λ is the multilayer period. By fitting our experimental data to the model

imposed by the equations 7.2 and 7.3, one obtains a critical angle of 0.31° and a multilayer period of 16.0 nm, which corresponds to a total thickness of 240 nm and agrees with the thickness value obtained from the TEM micrograph. Figure 7.13 depicts the fitting of the major peaks to the modified Bragg's law.

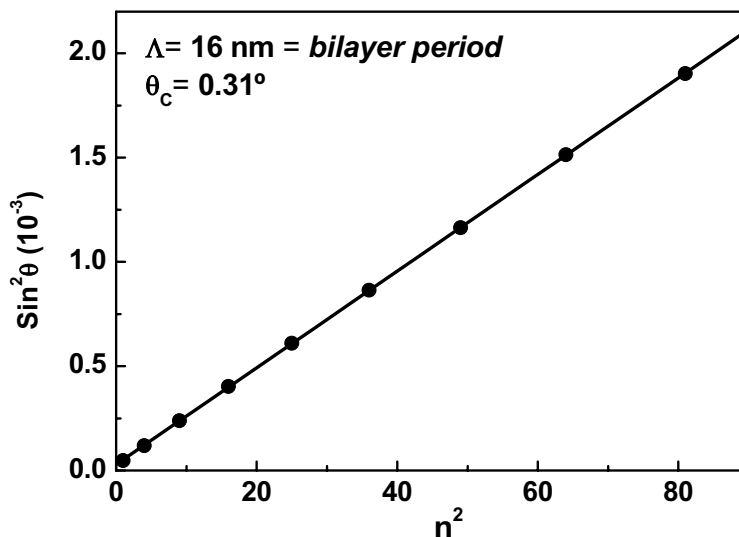


Figure 7.13: Modified Bragg's law fitting of major peaks shown in XRR diffractogram of figure 7.12.

This method constitutes XRR as an easy, very accurate (only depending on λ of the incident beam), and non-destructive technique to evaluate the multilayer period of samples, in comparison with the more laborious TEM analysis. However, it should be stated that the reliability of the XRR results depends on many factors: quality of interfaces, extended periodicity and enough contrast in mass densities.

These characteristics, along with control of the thickness and the combination of appropriate materials, allows the design of soft X-ray mirrors and high-reflecting thin films with potential uses, among others, in microelectronics, X-ray microscopy and X-ray photoemission spectrometry [Kondrashov P.E., 1998]. In these devices, and according to equations 7.2 and 7.3, the multilayer period should be matched to the incidence angle to obtain the Bragg reflection for a certain wavelength.

Additional W/a-C multilayers with smaller wavelength were deposited and characterised by XRD. Their bilayer thickness was set down to 1.0 nm, as shows table 7.3. Thus, Bragg peaks of the superlattice spectrum appear more separated along the 2θ scan (figure 7.14).

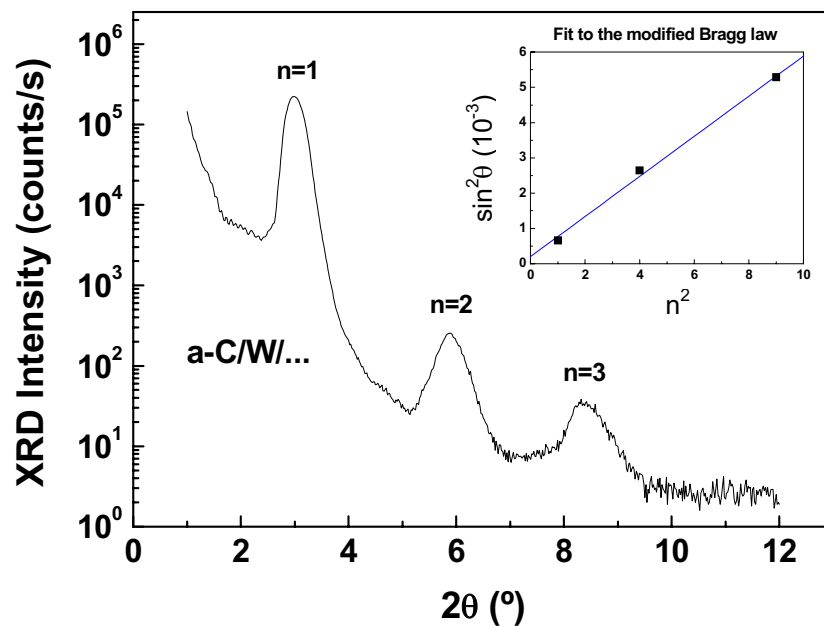


Figure 7.14: Plot of the XRR diffractogram corresponding to a W/a-C multilayer structure of 30 bilayers (PM 11-1). In the inset graph there is represented the modified Bragg-law fitting of the superlattice peaks from LAXRD diffractograms.

The high resolution XRR scan in figure 7.15 shows an additional spectrum modulation in the gap between two Bragg peaks. This superimposed modulation can be also observed in the inset of figure 7.12, and appears more defined in figure 7.15 due to the shorter multilayer wavelength. These structures are called Pendellösung fringes [Agarwal B.K., 1979], and are attributable to the finite extension of the structure.

The number of fringes per gap corresponds to $m-1$, where m is the number of bilayers. Although it is not possible to distinguish all the fringes, this number can be confirmed by relating their angular separation to the distance between two peaks. As a consequence, it is easy to understand that a non-limited multilayer would provide a XRR spectrum without Pendellösung fringes, i.e. clean inter-peak gaps.

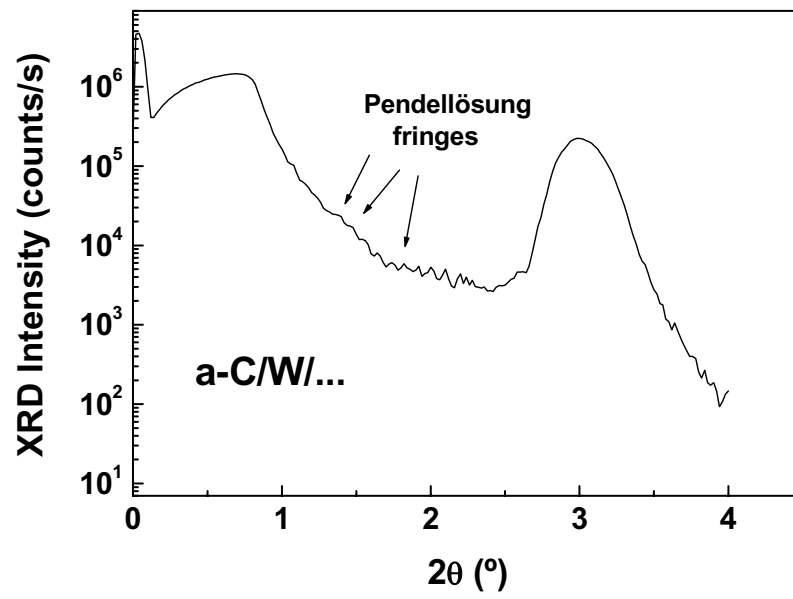


Figure 7.15: LAXRD plots of the first two peaks evidencing the Pendellösung fringes for W/a-C multilayers.

7.6. Mechanical properties

7.6.1. Intrinsic stress

Figure 7.16 shows that the compressive stress of DLC films is reduced from 2 to 0.3 GPa with increasing pressure. This stress lowering is in agreement with the correlation found in Mounier and Pauleau between the intensity of the intrinsic stress and the flux energy of C atoms and Ar ions impinging on the growing DLC film [Mounier E., 1996]. Indeed, the *peening* phenomena due to energetic particles impinging the film surface lead to the development of compressive intrinsic stress.

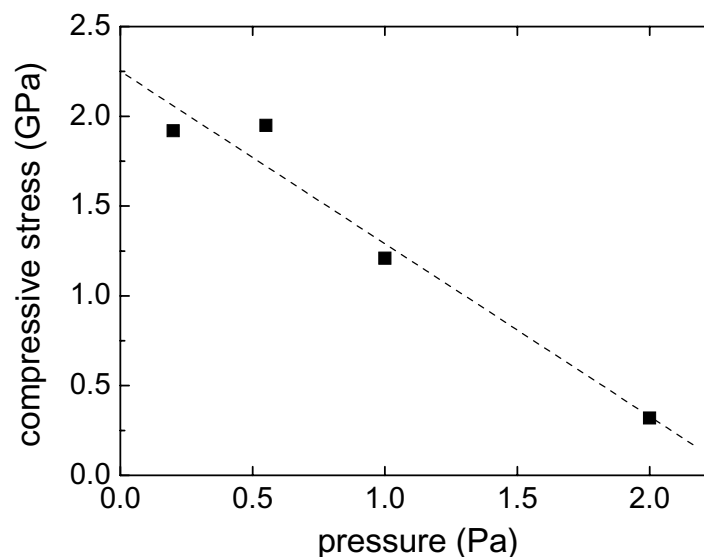


Figure 7.16: Dependence of compressive stress of DLC films on Ar pressure at 300 W of RF power.

The variation of the compressive stress with respect to the RF power is observed in figure 7.17. At low RF power (100-130 W) the compressive stress is above 3 GPa, whereas at higher RF power (150-300 W) its value is reduced to approximately 2 GPa. In SQWM mode, the compressive stress experiences a linear decrease until reaching a value of 1 GPa at the highest RF power.

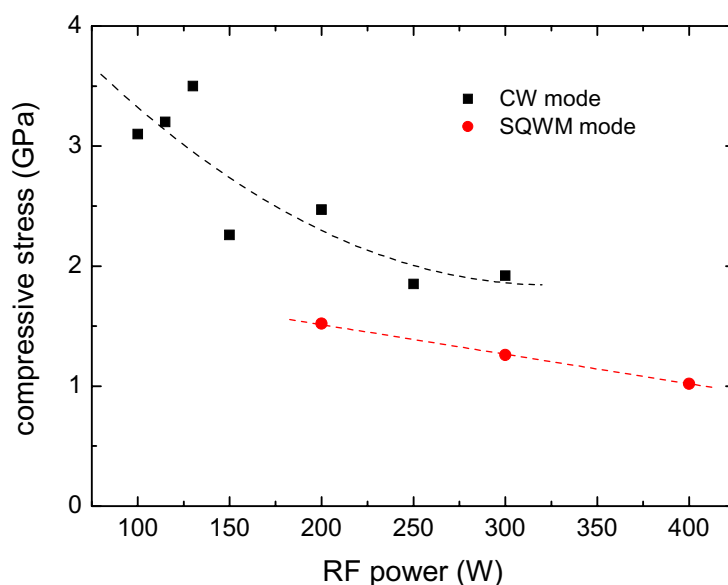


Figure 7.17: RF power dependence of compressive stress for DLC films grown either in CW or SQWM mode (RF power peak) at a fixed pressure of 0.2 Pa.

From the above results, we can infer that films grown at low RF power are more stressed than those obtained at higher RF power under more energetic conditions and with higher deposition rates.

Among the effects induced by pulsing the RF glow discharge, there is the enhancement of the electron density during the plasma-ON periods, and the lack of energetic bombardment on both the target and the substrate during the plasma-OFF periods. This latter effect allows the lowering of substrate temperature and, moreover, the relaxation of adsorbed carbon atoms on the growing surface, which can account for the reduction in compressive stress for the films grown under SQWM conditions in comparison with those deposited in CW discharges. The reduction in clustering of sp^2 phase pointed out in section 7.2 can be also explained in this way.

Table 7.4 lists values of the thickness and mechanical properties of W and DLC single layers. On the other hand, table 7.5 shows the parameters corresponding to the deposited W/a-C multilayer structures. When analysing the compressive residual stress of W/a-C multilayers, we find in table 7.5 that stress has decreased if compared to stress values of W and a-C single layers.

Sample	Mode	Thickness (nm)	Growth rate (nm/min)	Stress (GPa)	Hardness (GPa)	Reduced Young's Modulus (GPa)	Critical scratch load (mN)	Friction coefficient
W	CW	380	13	1.5	22.2	338	1880	0.07
a-C	SQWM	150	3	1.6	13.3	136	380	0.03
a-C	CW	140	4	2.0	12.6	122	370	0.03

Table 7.4: Parameters and mechanical properties of W and DLC single layers.

Sample	Mode	Total thickness (nm)	Stress (GPa)	Hardness (GPa)	Reduced Young's Modulus (GPa)	Critical scratch load (mN)	Friction coefficient
W/a-C	CW	200	1.5	15.8	162	-	-
W/a-C PM-1	SQWM	240	0.9	16.0	157	-	-
W/a-C PM-2	SQWM	180	1.3	16.2	177	-	-
W/a-C PM-3	SQWM	120	1.1	17.9	191	712	0.05
W/a-C PM 11-0	SQWM	85	-	-	-	-	-
W/a-C PM 11-1	SQWM	96	0.9	-	-	8000	-
W/a-C PM 12-1	SQWM	70	0.7	-	-	6000	-
W/a-C PM 12-2	SQWM	37	2.2	-	-	-	-
W/a-C PM 12-3	SQWM	30	3.7	-	-	6000	-
W/a-C PM 12-4	SQWM	52	2.8	-	-	-	-
W/a-C PM 12-5	SQWM	79	-	-	-	-	-

Table 7.5: Parameters and mechanical properties of multilayers composed of 15 (first four) and 30 (the rest) W/a-C bilayers. The thickness of each W layer in the first four W/a-C structures was 4 nm.

Though the deposition of DLC in SQWM mode supposes a decrease from 2.0 to 1.6 GPa in compressive stress, multilayer structures can be prepared so that stress becomes below 1 GPa (PM 11-1 and PM 12-1). The trend of critical load enhancement as the multilayer period decreases is remarkable. Concretely, sample PM 11-1 showed a resistance to fail up to 8 N.

These results are in concordance with recent research in hard coatings based on multilayer films composed of two different materials. These studies have shown that multilayer structures having the modulation period reduced to the order of 10 nm exhibit improved mechanical properties [Musil J., 2000] [Logothetidis S., 2000]. Furthermore, it seems that the stress is not homogeneously distributed within the whole multilayer system, since the structures of less than 52 nm thickness are the most stressed ones. It seems that the most surface layers are an important source of stress enhancement in W/a-C multilayers.

7.6.2. Hardness

The hardness and elastic modulus values of the DLC films (table 7.4) are similar to those reported for sputter-deposited films under no substrate bias conditions [Jacobsohn L.G., 1999], with low values of friction coefficient. Regarding W films, the measurements of hardness and elastic modulus resulted in slightly higher values than other results reported for 100-nm-thick W films grown on stainless steel substrates [Geyang L., 2001]. This difference in results may be a consequence of using a greater thickness and the influence of the c-Si substrate.

The hardness and elastic modulus values of W/a-C multilayers were between those of W and a-C single layers, and increased up to 18 GPa as the bilayer thickness was reduced to 8 nm (PM-3). Nanoindentation essays were not performed to films thinner than 100 nm because their results would include information from the substrate.

Now, we are interested in relating structural parameters of the multilayers with their mechanical properties. A well-known result from polycrystalline materials research is the Hall-Petch relation, which relates the yield stress, σ_y , of a polycrystalline solid to its grain diameter, d , as explained in chapter 1. This result explains the variations of yield strength in terms of dislocation motion among grain boundaries. Since dislocation propagation is hindered by grain boundaries, dislocation pileups are formed behind these obstacles and plastic yield of the material may occur.

A similar pileup against interlayer interfaces has been observed in multilayers. Recent investigations have led to a scaling theory of the Hall-Petch relation for multilayers [Friedman L.H., 1998]:

$$\sigma_y = Kd^{-a} + \sigma_0 \quad (7.4)$$

where σ_0 is a constant offset, K is a constant, and the exponent a is not necessarily equal to 1/2. In this theory, the distance d gives the bilayer thickness. Figure 7.18 plots hardness vs. multilayer period (wavelength) for the multilayers PM-1, -2 and -3, which are only distinguishable by their wavelengths. As expected from equation 7.4, their hardness decreases monotonically with the multilayer period.

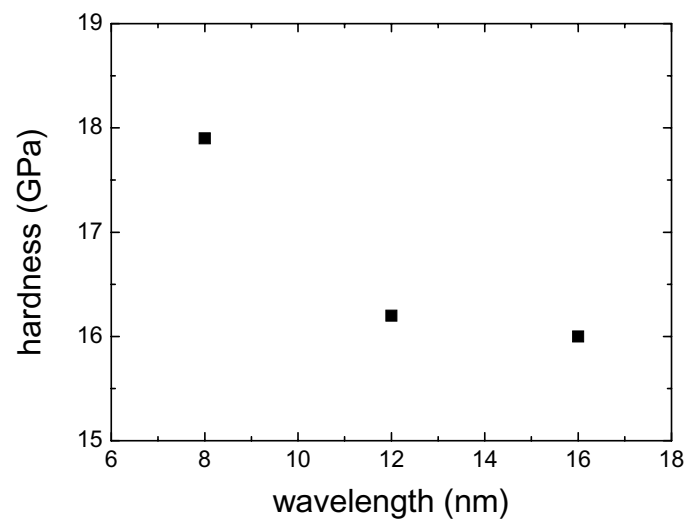


Figure 7.18: Evolution of hardness as a function of multilayer wavelength. Samples: PM-1, -2 and -3.

7.6.3. Friction

The tribological properties of DLC films were studied by scratching with a spherical-tip diamond indenter of 100 μm diameter. The microscratch results from tables 7.4 and 7.5 show a good adhesion either for W and DLC monolithic films. Moreover, the microscratch performed to sample PM-3 suggested an improvement in adherence to the substrate in the multilayer coatings, as revealed by the enhancement of the critical scratch load in comparison with that of single layer DLC films having similar thickness. The friction coefficient value was 0.05, which is intermediate between those of W single layer and DLC films.

Summary and conclusions

- 1) Multilayer W/a-C coatings with regular bilayer structure were prepared at room temperature by sequential RF magnetron sputtering using graphite and W targets, either in continuous wave or square-wave modulated mode.
- 2) XRR and TEM analyses accounted for the formation of multilayered structures with sharp interfaces and a well-defined multilayer period.
- 3) Their characterisation indicates the following improvements in the mechanical properties with respect to the a-C single layers: lowering of the compressive stress, better adherence to the substrate, and increase in hardness and elastic modulus. These results open the possibility of using W/a-C structures as protective coatings.
- 4) The multilayer films studied may also find applications in soft X-ray reflecting systems due to their high X-ray reflectance.